TSL/ISV-96-0137
April 1996

ISSN 0284-2769

Signals for Intrinsic Charm in High Energy Interactions

G. Ingelman[a,b,1] and M. Thunman[a,2]

[a] Dept. of Radiation Sciences, Uppsala University, Box 535, S-751 21 Uppsala, Sweden
[b] Deutsches Elektronen-Synchrotron DESY, Notkestrasse 85, D-22603 Hamburg, Germany

Abstract: The prospects to test the hypothesis of intrinsic charm quarks in the proton are investigated. We consider how this component can be directly or indirectly probed in deep inelastic scattering at HERA and in fixed target experiments and find that an overlooked signal might be present in existing NMC data. Applying the intrinsic charm model to hadron collisions we compare the resulting charm production cross-sections with those based on standard perturbative QCD and available data. Extrapolating to higher energies we obtain predictions for charm production at the Tevatron and LHC.

1 Introduction

The hypothesis of intrinsic charm quarks in the proton was introduced [1] as an attempt to understand a large discrepancy between early charm hadroproduction data and leading order perturbative QCD (pQCD) calculations. The data from ISR (see refs. in [1]) were about an order of magnitude higher than the prediction and had a rather flat distribution in longitudinal momentum compared to the sharp decrease with Feynman $x_F = p_\parallel/p_{max}$ expected from pQCD. As more data have been collected at different energies and next-to-leading order (NLO) pQCD calculations have been made, the discrepancy has largely disappeared. Still, however, there are certain aspects of the data which are difficult to understand within the pQCD framework, but are natural if the intrinsic charm hypothesis is basically correct. This concerns the mentioned x_F distributions of leading charm in hadroproduction [2, 3], the dependence on the nuclear number (A^α) of J/ψ production [4] and double J/ψ production [5].

Thus, although the main features of charm production can now be understood by conventional pQCD, certain aspects of the data indicate the presence of some additional mechanism. Intrinsic charm may be such a process, which gives a small contribution to the inclusive cross section but could dominate in some regions of phase space.

The hypothesis of intrinsic charm (IC) amounts to assuming the existence of a $c\bar{c}$-pair as a non-perturbative component in the bound state nucleon [1]. This means that the Fock-state decomposition of the proton wave function, $|p\rangle = \alpha|uud\rangle + \beta|uudc\bar{c}\rangle + ...$, contains a small, but finite, probability β^2 for such an intrinsic quark-antiquark pair. This should be viewed as a

[1] ingelman@tsl.uu.se
[2] thunman@tsl.uu.se

quantum fluctuation of the proton state. The normalization of the heavy quark Fock component is the key unknown, although it should decrease as $1/m_Q^2$. Originally, a 1% probability for intrinsic charm was assumed, but later investigations indicate a somewhat smaller but non-vanishing level; $\sim 0.3\%$ [6] and $(0.86 \pm 0.60)\%$ [7].

Viewed in an infinite momentum frame, all non-perturbative and thereby long-lived components must move with essentially the same velocity in order that the proton can 'stay together'. The larger mass of the charmed quarks then implies that they take a larger fraction of the proton momentum. This can be quantified by applying old-fashioned perturbation theory to obtain the momentum distribution [1]

$$P(p \to uudc\bar{c}) \propto \left[m_p^2 - \sum_{i=1}^{5} \frac{m_{\perp i}^2}{x_i} \right]^{-2} \tag{1}$$

in terms of the fractional momenta x_i of the five partons i in the $|uudc\bar{c}\rangle$ state. The probability β^2 of this state is related to the normalisation N_5 of ref. [1]. Neglecting the transverse masses ($m_\perp^2 = m^2 + p_\perp^2$) of the light quarks in comparison to the charm quark mass results in the momentum distribution

$$P(x_1, x_2, x_3, x_c, x_{\bar{c}}) \propto \frac{x_c^2 x_{\bar{c}}^2}{(x_c + x_{\bar{c}})^2} \delta(1 - x_1 - x_2 - x_3 - x_c - x_{\bar{c}}) \tag{2}$$

where the (transverse) charm quark mass is absorbed into the overall normalisation. This function favours large charm quark momenta as anticipated. In fact, one obtains $\langle x_c \rangle = 2/7$ by integrating out the remaining degrees of freedom x_i.

An intrinsic $c\bar{c}$ quantum fluctuation can be realised through an interaction, such that charmed particles are created. In proton-proton collisions this could certainly happen through a hard interaction with such a charm quark, but the cross section is then suppressed both by the small probability of the fluctuation itself and by the smallness of the perturbative QCD cross section. The charm quarks may, however, also be put on shell through non-perturbative interactions that are not as strongly suppressed [8]. Deep inelastic lepton-proton scattering would be another possibility, where this intrinsic charm component could be more directly probed. To investigate these possibilities we have constructed a model based on refs. [1, 4, 9]. In part we use Monte Carlo techniques to simulate explicit events giving a powerful method to extract information on various differential distributions.

One may also consider the extension from intrinsic charm to intrinsic bottom quarks. Since the overall probability scales with $1/m_Q^2$, one expects all cross sections for intrinsic bottom to be about a factor ten lower. The x-distributions for bottom quarks should be somewhat harder than for charm, but since light quark masses have already been neglected in Eq. (2) it also applies for intrinsic bottom and the same distribution as for charm is obtained in this approximation.

In section 2 we investigate IC in deep inelastic scattering (DIS) in fixed target and collider mode. In the former, we explicitly consider the experiment New Muon Collaboration (NMC) at CERN and find that an interesting number of intrinsic charm events could be present in their data samples. For ep collisions in HERA, we extend a previous study [10] to include the possibility of scattering on a light quark such that the intrinsic charm $c\bar{c}$-pair is freed and give charmed particles in the forward proton remnant direction. The case of hadronic charm production is studied in section 3. The measured charm production cross sections are compared to those calculated in pQCD to constrain the allowed amount of IC. Here, an important issue is the energy dependence of the cross section for IC, where two alternatives are considered. Based on this, we provide differential distributions of charm production from IC in comparison

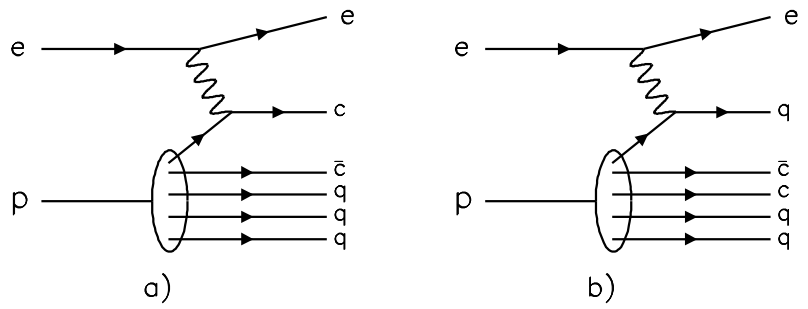

Figure 1: *Deep inelastic scattering on a proton containing an intrinsic $c\bar{c}$-pair; a) scattering on the charm quark, b) scattering on a light valence quark.*

to the standard pQCD treatment, as applied to the Tevatron and LHC. Finally, section 4 gives a concluding discussion.

2 Intrinsic charm in deep inelastic scattering

2.1 General framework

In DIS it should be possible to measure the effective IC parton density by direct scattering on an intrinsic (anti)charm quark (Fig. 1a). The parton density is obtained from Eq. (2) by integrating out all degrees of freedom except the momentum fraction x of the charm quark (or antiquark), resulting in

$$c_{IC}(x) = \beta^2 1800 x^2 \left\{ \frac{1}{3}(1-x)(1+10x+x^2) + 2x(1+x)\ln x \right\} \tag{3}$$

The DIS charm cross section is given by

$$\frac{\mathrm{d}^2\sigma}{\mathrm{d}x\mathrm{d}Q^2} = \frac{2\pi\alpha}{xQ^4}\left[1+(1-y)^2\right]\, F_2^c(x,Q^2) \tag{4}$$

in terms of the conventional DIS variables; Bjorken $x = Q^2/2P\cdot q$, $y = P\cdot q/P\cdot p_\ell$ where P, p_ℓ is the momentum of the initial proton and lepton, and q is the four momentum transfer of the exchanged photon. Only photon exchange contribution is here included since the high-Q^2 region with Z^0 exchange contributions can be neglected in our applications. The general charm structure function is

$$F_2^c(x,Q^2) = e_c^2\, \left\{ xc(x,Q^2) + x\bar{c}(x,Q^2) \right\} \tag{5}$$

and F_2^{IC} is obtained if the intrinsic charm quark density $c_{IC}(x,Q^2)$ is used. The Q^2 dependence from normal leading log GLAP equations have been calculated for IC in [6], but can be taken into account through a simple extension of the parameterisation in Eq. (3) [10].

We have included an option to treat DIS on intrinsic heavy quarks in the Monte Carlo program Lepto [11] using this formalism and are therefore able to simulate complete events based on this IC model. As for normal DIS events, higher order perturbative parton emissions from the incoming and scattered quark are included through parton showers. Hadronisation and particle decays are then performed according to the Lund model [12] in its Monte Carlo implementation Jetset [13].

In addition to this direct scattering on an intrinsic charm quark, one may also consider the case of DIS on a light (valence) quark (Fig. 1b) such that the intrinsic $c\bar{c}$-pair in the proton is 'liberated' and give charmed particles in the phase space region corresponding to the 'spectator' proton remnant. To simulate this case also, we have made add-on routines to LEPTO based on the following simple model. The normal electroweak DIS cross section is first used to treat the basic scattering on a light quark. The corresponding quark density function is here obtained from Eq. (2) by integrating out all degrees of freedom, except x_1 for the light (valence) quark to scatter on,

$$q_{IC}(x_1) = \beta^2\, 6\,(1-x_1)^5. \tag{6}$$

The probability β^2 of the $|uudc\bar{c}\rangle$ state is included here and gives the normalisation of the cross section for this intrinsic charm process.

From the remaining $qqc\bar{c}$ system, one then considers the production of $\bar{D}$-mesons, Λ_c and J/ψ through a coalescence [4, 9] of the relevant partons in Fig. 1b. The longitudinal momentum distributions for these charmed particles are obtained, for a given x_1, by integrating over the other momentum fractions in Eq. (2) and inserting a δ-function for the particle to be produced, *i.e.* $\delta(x_{\bar{D}} - x_q - x_{\bar{c}})$, $\delta(x_{\Lambda_c} - x_u - x_d - x_c)$ or $\delta(x_{J/\psi} - x_c - x_{\bar{c}})$. Considering momentum fractions relative to the proton remnant, *i.e.* after x_1 is removed, corresponds to the variable substitution $x \to \xi = x/(1-x_1)$. This gives expressions that factorise into an x_1-dependent part and a ξ-dependent part. Since x_1 is already chosen, the former part can be absorbed into the normalisation of the ξ-distribution. Thus, normalising to overall unit probability, one obtains the probability distributions

$$\begin{aligned}
\frac{\mathrm{d}N_{\bar{D}}}{\mathrm{d}\xi} &= P_{\bar{D}}\ 300\ \Big\{\ \xi^4\ln\xi\ +\ (1-\xi)^4\ln(1-\xi)\ + \\
&\qquad \xi\,(1-\xi)\,[\xi^2 - \frac{1}{2}\xi(1-\xi) + (1-\xi)^2] \qquad \Big\} \qquad (7)\\
\frac{\mathrm{d}N_{\Lambda_c}}{\mathrm{d}\xi} &= P_{\Lambda_c}\ 300\ (1-\xi)^2\ \Big\{\xi\,[\,6\ -5\xi\,]\ +2\,[\,\xi^2\ +\ 4\xi\ +\ 3\,]\ \ln(1-\xi)\Big\} \qquad (8)\\
\frac{\mathrm{d}N_{J/\psi}}{\mathrm{d}\xi} &= P_{J/\psi}\ 20\ (1-\xi)\,\xi^3 \qquad (9)
\end{aligned}$$

where $P_{\bar{D}}, P_{\Lambda_c}$ and $P_{J/\psi}$ are the relative probabilities to form the three different charmed particles. These distributions are illustrated in Fig. 2.

The overall normalisation is already accounted for (by β^2) in the DIS cross section and only the relative probabilities $P_{\bar{D}}$, P_{Λ_c} and $P_{J/\psi}$ need to be specified. Following the investigations in [4, 9] for the similar case in hadroproduction, we take 66% $\overline{D}$, 33% Λ_c/Σ_c and 1% J/ψ. In each case there is a remaining parton in the proton remnant, *i.e.* a qc diquark, a $\bar{c}$ quark and a qq valence diquark, respectively. These are all anti-triplets in colour and are connected with a Lund string to the scattered quark to form a singlet system that hadronises using the normal Lund model. Note, that the charm (anti)quark at the proton remnant end of the string also gives rise to a charmed hadron. Before hadronisation, however, the scattered quark may radiate partons as treated by parton showers in LEPTO.

In the following, we extend the previous study [10] of direct DIS on IC in two ways. First, a more dedicated study of direct IC scattering in connection with the New Muon Collaboration (NMC) experiment is made. Secondly, we consider the above model for indirect IC scattering applied to ep collisions at HERA and compare with direct IC scattering as well as conventional boson-gluon fusion into $c\bar{c}$ from pQCD.

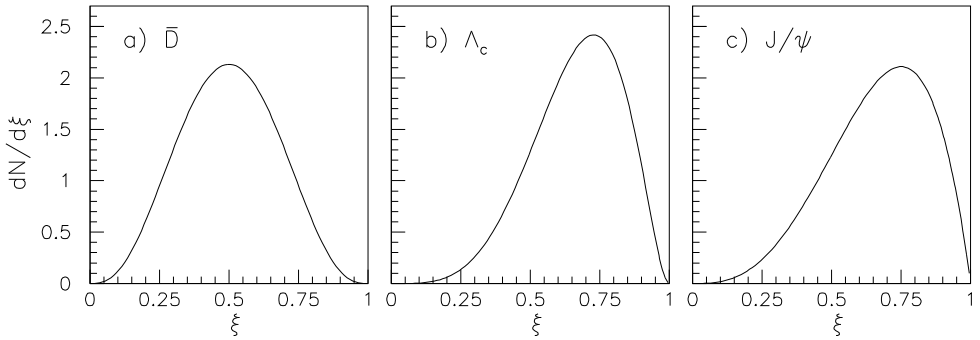

Figure 2: *Distribution of rescaled longitudinal momentum $\xi = x/(1-x_1)$ of (a) $\bar{D}$-mesons, (b) Λ_c and (c) J/ψ produced through coalescence in the remnant system from a DIS scattering on a valence quark in the intrinsic charm $|uudc\bar{c}\rangle$ state. The distributions shown in the scaled variable are normalised to unit integral as discussed in the text.*

2.2 Fixed target muon scattering (NMC)

In case of fixed target experiments the interest is focused on the direct scattering on intrinsic charm. This gives a high energy charmed particle in the current direction. The resulting high energy muon from a semi-leptonic decay can then be used as a signal for charm. In the indirect IC process, however, the charmed particles will emerge in the target region and resulting muons will have low energy and hence be more difficult to identify. Therefore we will not consider this indirect mechanism in the fixed target case.

We thus concentrate on the direct scattering on intrinsic charm quarks and use our Monte Carlo model to simulate events corresponding to the NMC experimental situation. This means having a $280\,GeV$ muon beam on a stationary proton target and applying the cuts $Q^2 > 2\,GeV^2$ and $W^2 > 100\,GeV^2$.

From the simulated intrinsic charm events we extract the structure function F_2^{IC}, using Eq. (4), resulting in the three curves in Fig. 3 for different intrinsic charm probabilities. For comparison, we have calculated F_2^c arising from the conventional boson-gluon fusion (BGF) process $\gamma^* g \to c\bar{c}$. This was obtained from a similar Monte Carlo simulation using the AROMA program [14], which is an implementation of this process using the leading order pQCD matrix elements with the proper charm quark mass effects included (together with parton showers and hadronisation as in LEPTO). The large-x feature of IC is clearly seen and results in a dominance of IC over pQCD at large enough x. The cross-over point depends on the unknown absolute normalisation of IC as illustrated.

One should here consider the experimental information on the inclusive F_2^c available from the European Muon Collaboration (EMC). Their original analysis gave an upper limit for IC (β^2) of 0.6% at 95% CL [15]. In a later analysis [6], the QCD evolution of the IC structure function, as mentioned above, and charm mass effects were taken into account giving positive evidence for IC at the level 0.3%. A very recent investigation [7] (in parallel with our study) has improved the theoretical treatment by including next-to-leading order corrections both for the IC and pQCD processes. Based on the same EMC data they find that an intrinsic charm contribution of $(0.86 \pm 0.60)\%$ is indicated (in the bin of large energy transfer with mean $\nu = 168\,GeV$).

Thus, there is some evidence for IC from the inclusive F_2^c measurement of EMC, but it is not conclusive. One therefore needs to consider whether further information can be obtained.

The success of the experimental method to tag charm through muons depends very much on

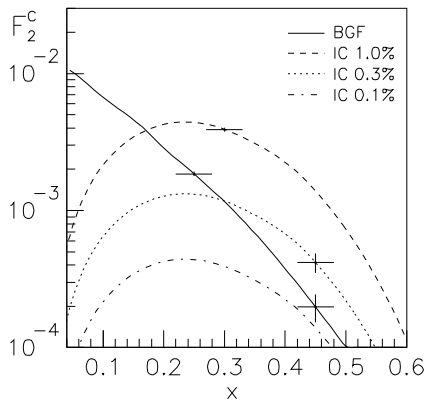

Figure 3: *The charm structure function $F_2^c(x)$ obtained from our Monte Carlo simulation of DIS on intrinsic charm quarks, with the different indicated normalisations (β^2), and the conventional pQCD boson gluon fusion process $\gamma^* g \to c\bar{c}$ (solid curve). The error bars indicate the potential statistical precision of the discussed NMC data sample.*

the amount of muons from other sources. The background to IC from perturbatively produced charm, as given above, is in a sense an irreducible background. There is, however, also a severe background from the decays of light hadrons, mostly pions and kaons, that are copiously produced. Since these particles have a much longer life-time than charm, their effect can be reduced by either having the muon detectors close to the target or having hadron absorbers to filter out the prompt muons.

The normal experimental arrangement of NMC is to have little material between the target and the detectors. This implies, however, a substantial muon background from π and K decays. However, in some runs of the NMC experiment a set-up more suitable for a charm search was used. In the heavy target configurations during 1987-88 there were hadron absorbers immediately downstream of the targets. We have developed an analytic method to calculate the suppression of this muon background due to the hadron absorption. The details are reported in [16], where it is also applied to this NMC set-up. Thus, we calculate the development of the flux of produced mesons within the targets, in the calorimeters/absorbers and in the empty space between these elements. The resulting muon flux from hadron decays was found to be reduced to only $\sim 6\%$ of the flux without such absorption. In addition, we found that the calorimeter between the target and the absorber could also be used as a target. Charmed hadrons can also be absorbed, but due to their much shorter life-time the effect is negligible. For example, the decay length of a $D^{\pm}$ is at most $\sim 1/10$ of its interaction length (corresponding to a momentum of $180\,GeV$, which is about the highest to be expected).

An experimentally realistic study of signal and background muons has been performed using Monte Carlo simulations. The results are displayed in Fig. 4. The background from light hadron decays was obtained by applying the above suppression factor on the yield from simulated normal DIS events. Here, the standard version of LEPTO was used in the same kinematic region as specified above. The muons from IC and the pQCD process are obtained with our modified LEPTO version and AROMA, respectively.

The resulting energy spectra of muons are shown in Fig. 4 for three sets of cuts. Fig. 4a is for the above mentioned standard cuts; $Q^2 > 2\,GeV$ to ensure DIS and $W^2 > 100\,GeV^2$ to have enough energy in the hadronic system for charm pair production. Fig. 4b have extra cuts motivated by the NMC experiment; the scattered muon in the energy range $42 < E_{\mu 1} < 224 GeV$

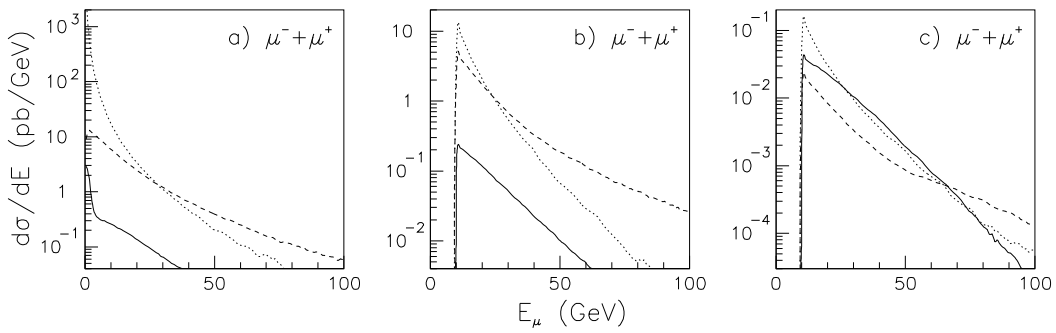

Figure 4: *Differential cross section versus energy of muons ($\mu^- + \mu^+$) from the decay of charmed particles originating from a 1% intrinsic charm component in the proton (solid curves), from pQCD $\gamma^* g \to c\bar{c}$ (dashed curve) and from decay of light mesons (mainly π, K) (dotted curves); all in 280 GeV muon-proton scattering with cuts: (a) $Q^2 > 2\,GeV$ and $W^2 > 100\,GeV^2$, (b) NMC cuts on the scattered muon $42 < E_{\mu 1} < 224\,GeV$ and $\theta > 10\,mrad$ and on secondary muons $E_{\mu 2} > 10\,GeV$, (c) $E_{\mu 1} > 100\,GeV$ and $x_{Bj} > 0.2$ to enhance IC. An overall reduction for muons from π and K decays to 6% has been applied to account for the discussed hadron absorption effect in NMC.*

and at angle $\theta > 10\,mrad$ to emerge from the beam and secondary muons (from other sources) having a large enough energy $E_{\mu 2} > 10\,GeV$ to be indentified. In Fig. 4c the additional cuts $E_{\mu 1} > 100\,GeV$ and $x_{Bj} > 0.2$ were also made to identify the highest energy muon as the scattered one and select the large-x region. This last requirement is ment to enhance intrinsic charm events over the background processes (*cf.* Fig. 3). As demonstrated, it is then possible get muons from IC to the same level as the backgrounds.

With the additional cuts the absolute rate is lowered such that large statistics data samples are needed. This may be satisfied by the NMC run in 1988 when data were collected for $9.5 \cdot 10^{11}$ muons of $280\,GeV$ on four targets of thickness $145\,g/cm^2$ each, which corresponds to an integrated luminousity of $334\,pb^{-1}$. The statistical precision that can be expected in F_2^c for this sample is illustrated in Fig. 3 for a few x-bins. This should give ~ 200 events with muons ($\mu^- + \mu^+$) of energy larger than $10\,GeV$ and fulfilling the stricter set of cuts, *i.e.* corresponding to the integrated distribution in Fig. 4c. In the same way one obtains ~ 85 muons from charm produced by the pQCD process and ~ 340 muons from π, K decays after the hadron absorpion reduction as estimated with the above mentioned analytic method. Additional data based on $8.4 \cdot 10^{11}$ muons of $200\,GeV$ energy could also be analysed in this way.

In order to reduce the background from π, K decays further, one might also use secondary vertices based on the difference in decay length of light mesons as compared to charmed particles. We have investigated [16] this by considering the impact parameter of the muon tracks with respect to the primary interaction vertex. The impact parameter for muons from charm is always less than $0.5\,cm$, whereas it is typically larger for those from light mesons. However, the hadron absorbers that reduce the rate of muons from light mesons, also give rise to multiple scattering of the muons passing through. This causes a smearing of the reconstructed impact parameter which we find [16] has a Gaussian distribution of width $3.5\,cm$. Thus, the *measureable* impact parameter of muons from charm does not seem to provide a useable signature, although a safe conclusion would require a detailed simulation of the experimental conditions.

In these estimates for IC we have assumed a 1% normalisation (β^2) of the IC component and leave a trivial rescaling to any smaller value that may be preferred. Based on the above,

we conclude that it seems possible to find an intrinsic charm signal down to the 0.2% level in the NMC data through an excess of muons as compared to the expected background (*e.g.* an excess of about 40 over a background of 425 muons). The same sensitivity can be estimated from the precisions of F_2^c as shown in Fig. 3. The determination of the BGF background is here essential, but uncertainties in the overall normalisation of the theoretical calculation can be well determined at small-x where this process dominates F_2^c and the statistical precision is high.

One should note that at large Q^2, the intrinsic and extrinsic (BGF) charm processes have different scaling behaviour with the charm quark mass; $1/m_c^2$ and $log(m_c^2)$, respectively. This can give an additional handle to separate them in a data sample.

2.3 Electron-proton collider

In HERA at DESY, 30 GeV electrons (or positrons) are collided with 820 GeV protons. The direct DIS on intrinsic charm quarks in the proton has been investigated previously [10]. Since the intrinsic charm quark typically has a large x, it will be scattered at a rather small forward angle close to the proton beam direction. This makes it difficult to detect muons from semileptonic decays and only a fraction of the events are observable. For details we refer to [10].

The above discussed case of indirect intrinsic charm scattering may also occur. The charm particles are then produced in the forward-moving proton remnant system and will emerge in the very forward direction and therefore be hard to detect. Still, it is worthwile to estimate the rate and the distribution in pseudo-rapidity of the emerging muons.

In a recent paper [17] these different IC processes in ep collisions were discussed at a theoretical and qualitative level. Here, we concentrate on a phenomenological study of these processes

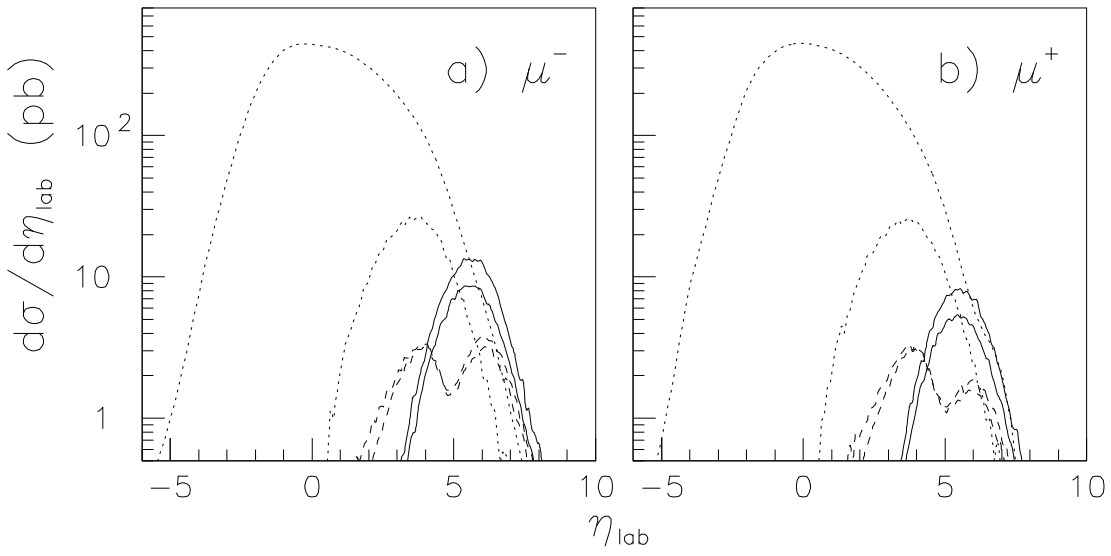

Figure 5: *Distribution in pseudorapidity ($\eta = -ln\ tan(\theta/2)$) for muons from semileptonic decays of charmed particles produced through different DIS processes at HERA: scattering on a light (valence) quark in the intrinsic charm proton state $|uudc\bar{c}\rangle$ (solid curves), direct scattering on an intrinsic charm state (dashed curves) and the conventional pQCD $\gamma^* g \to c\bar{c}$ process (dotted curves). In each case, the upper curve correspond to the inclusive event sample (see text) and the lower curve after the cuts $x > 0.03$, $y < 0.3$ made to suppress the pQCD contribution. (Note, $\eta > 0$ corresponds to the proton beam direction.)*

in order to get quantitative results for direct experimental considerations.

It is of obvious interest to compare the different charm production mechanisms, which can easily be made through our different Monte Carlo simulation programs as discussed above. Thus, we use the add-on to LEPTO to simulate the indirect IC scattering process, LEPTO for direct scattering on an intrinsic charm quark and AROMA for the pQCD $\gamma^* g \to c\bar{c}$ process. In all cases ep events at the HERA energy were simulated with $Q^2 > 4\,GeV^2$ and $W^2 > 100\,GeV^2$.

In Fig. 5 we display the resulting distributions in pseudo-rapidity for muons from charm decays in the different cases. As can be seen, the conventional pQCD process dominates strongly the overall rate, but can be substantially reduced by the simple cuts $x > 0.03$, $y < 0.3$ which hardly affects the IC contributions. The two IC processes give charm at large rapidities in the proton beam direction, as expected.

One may notice that the muon detectors in the HERA experiments only covers pseudo-rapidities up to $3 - 4$. A possibility would be to lower the proton beam energy and thereby decrease the strong forward boost effect. For example, lowering the proton beam energy to 300 GeV, would essentially shift the distributions lower in rapidity by about one unit. This has been investigated for the direct IC scattering in ref. [10], where also the background of muons from light meson decays (π, K) was studied.

Although it does not seems possible to detect these IC processes with todays set-ups in the H1 and ZEUS experiments, it is of interest for the upgrades under discussion, *e.g.* within the presently running workshop on 'Future Physics at HERA'.

3 Intrinsic charm in hadron interactions

We now turn to hadron collisions for which the intrinsic charm hypothesis was first developed [1]. Here also, one could consider to probe the intrinsic charm quarks in hard scattering processes such that pQCD is applicable. This would, however, result in a very low cross section; suppressed both by the IC probability and the smallness of the perturbative cross section. The charm quark may, however, also be put on shell and emerge in real charmed particles through softer non-perturbative interactions that are not strongly suppressed [8]. As in previous investigations of this subject [4, 9], we will consider the shapes of x_F distributions as derived from the IC model separately from the overall normalisation of the cross section. The energy dependence of the cross section is a non-trivial issue, which we discuss in connection with pQCD charm production and charm hadroproduction data.

3.1 Basic x_F distributions in IC

A non-perturbative hadronic interaction of a proton in an IC state is thus assumed to realise charmed hadrons. This may occur through conventional hadronisation in a similar way as when the charm quark and antiquark is produced in a hard interaction, *e.g.* in a hadron-hadron or e^+e^- collision. This can be well describe by a fragmentation model, like the Lund model [12], or a parametrised fragmentation function such as the Peterson function [18]. The effective charm fragmentation function is quite hard such that a simple approximation is to use a δ-function to let the charmed hadron get the same momentum as the charmed quark. Given the uncertainties of the intrinsic charm momentum distribution to be used as input for the fragmentation, this δ-function fragmentation is adequate here and has also been used in previous IC studies [3].

The charm (anti)quark may also coalesce with another quark or diquark from the same initial proton state $|uudc\bar{c}\rangle$ to form a hadron. This may happen when such a parton system forms a colour singlet, but has too small invariant mass to hadronise according to the Lund

model. Such a mechanism is especially important for the production of Λ_c, but should also play an important role in the production of D-mesons. For an initial proton, this gives an asymmetry between $\overline{D}$ mesons, which can be formed by this coalescence process, and D mesons which cannot. Such differences in leading particle spectra are observed experimentally (see [3] and references therein) and may be an indication for these mechanisms. The c and $\bar{c}$ can also coalesce to form a charmonium state, mainly J/ψ or some higher resonance that mostly decays into the lowest lying J/ψ state.

The relative probabilities for these processes are not known, but have been discussed before. Following [4, 9] we use the recombination probabilities 50% to form a $\overline{D}$-meson and 30% for a Λ_c. The probability to directly form a J/ψ (*i.e.* the $c\bar{c}$ pair is combined) is taken to be 1%. The absolute rates of Λ_c and J/ψ do, of course, depend strongly on these values. The D-meson rates and distributions are, however, not so sensitive to these values because the resulting distributions from fragmentation and coalescence are rather similar. The c or $\bar{c}$ quarks that do not coalesce with spectator partons, are hadronised to D-mesons with the mentioned δ-function. This is the case for the remaining c or $\bar{c}$-quark in events with coalescence and both c and $\bar{c}$ in the remaining 19% of events without coalescence.

The momentum of the hadron formed through coalescence is taken as the sum of the corresponding x_i's, *e.g.* $x_{\Lambda_c} = x_c + x_u + x_d$. The momentum distribution is then obtained by folding Eq. (2) with the proper δ function, *e.g.* $\delta(x_{\Lambda_c} - x_c - x_u - x_d)$, and integrating out all extra degrees of freedom. When the c or $\bar{c}$ quarks are hadronised with the δ-function, the D-meson takes the whole intrinsic charm quark momentum as given by Eq. (3). This procedure is consistent with low-p_t charm hadroproduction data [3].

Based on this model we then obtain the following correlated probability distributions in longitudinal momentum fraction (Feynman-x) for the different combinations of charmed hadrons in an event; a $D\,\overline{D}$ pair produced through fragmentation

$$\frac{\mathrm{d}P}{\mathrm{d}x_D\,\mathrm{d}x_{\bar{D}}} \propto 1800\ \frac{(1-x_D-x_{\bar{D}})^2 x_D^2 x_{\bar{D}}^2}{(x_D+x_{\bar{D}})^2}\,; \tag{10}$$

a D from fragmentation and a $\overline{D}$ from coalescence

$$\frac{\mathrm{d}P}{\mathrm{d}x_D\,\mathrm{d}x_{\bar{D}}} \propto 3600\ (1-x_D-x_{\bar{D}}) x_D^2 \left(x_D + x_{\bar{D}} - \frac{x_D^2}{x_D+x_{\bar{D}}} - 2x_D^2 \ln\frac{x_D+x_{\bar{D}}}{x_D^2} \right)\,; \tag{11}$$

a $\overline{D}$ from fragmentation and a Λ_c from coalescence

$$\frac{\mathrm{d}P}{\mathrm{d}x_{\Lambda_c}\,\mathrm{d}x_{\bar{D}}} \propto 3600\, x_{\bar{D}}^2 \left(\frac{x_{\Lambda_c}}{2} + 3\,x_{\bar{D}}\,x_{\Lambda_c} - x_{\bar{D}}\,(3\,x_{\bar{D}} + 2\,x_{\Lambda_c})\,\ln\frac{x_{\bar{D}}+x_{\Lambda_c}}{x_{\bar{D}}} \right)\,; \tag{12}$$

and a J/Ψ from coalescence

$$\frac{\mathrm{d}P}{\mathrm{d}x_{J/\psi}} \propto 20\,(1-x_{J/\psi})^2 x_{J/\psi}^3. \tag{13}$$

These two-dimensional distributions are plotted in Fig. 6. Each one is here normalised to unit integral and their relative weight are the percentages discussed. Obviously, the sum of the two x's in each case cannot exceed unity and the distributions therefore vanish when passing the diagonal in the two-dimensional plots. The J/ψ, formed by the coalescence of the $c\bar{c}$-pair, take a larger momentum fraction since it is formed of two quarks with relatively high x_F, as shown in Fig. 6. The Λ_c, which coalesce with two valence quarks, gets a larger momentum than the D mesons as demonstrated in Fig. 6.

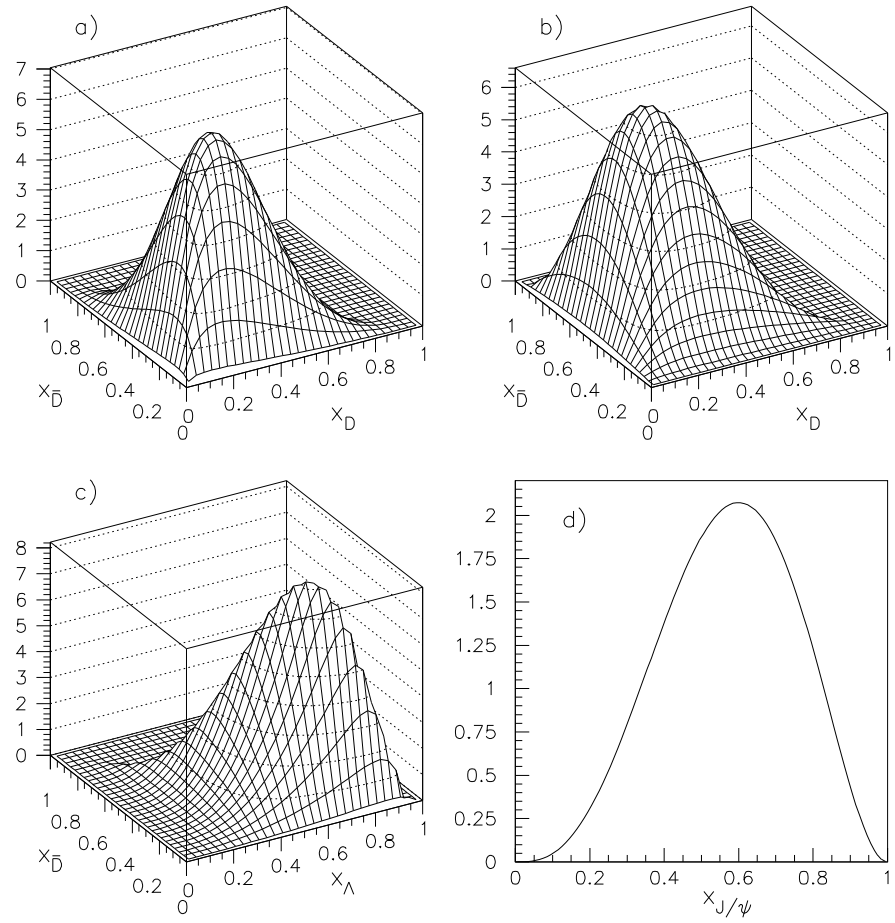

Figure 6: *Probability distributions $dP/dx_1 dx_2$ and $dP/dx_{J/\psi}$ in longitudinal momentum fractions (x_i) for charmed particles from IC: (a) $D\overline{D}$ from fragmentation, Eq. (10). (b) D from fragmentation and a $\overline{D}$ from coalescence, Eq. (11). (c) $\overline{D}$ from fragmentation and Λ_c from coalescence, Eq. (12). (d) J/ψ from coalescence, Eq. (13).*

In addition to these charmed particles, higher mass states may also be produced. However, these decay rapidly to the treated ones and can therefore be considered included in these parameterisations. D_s cannot be produced in the coalescence process, but is allowed in the fragmentation process although at a suppressed rate (*e.g.* by a factor ~ 7 in the Lund model). Since its spectrum would be essentially the same as the other D-mesons, we include it with them and use D as a generic notation for all pseudoscalar charm mesons. The vector mesons D^* decays strongly to D-mesons, but the decays are not charge symmetric; $D^{*0} \to D^0(100\%), D^{*\pm} \to D^0(68\%)/D^{\pm}(32\%)$. This effect is taken into account after having chosen a primary D^* or D from spin statistics.

The shapes of the x_F-distributions for charmed particles from intrinsic charm are thereby specified and found to be quite hard, as expected. In fact, they are harder than those for charm from perturbatively produced charm, as shown below. This gives a possibility that IC may contribute substantially or even dominate at large x_F, depending on the absolute normalisation of the production cross section.

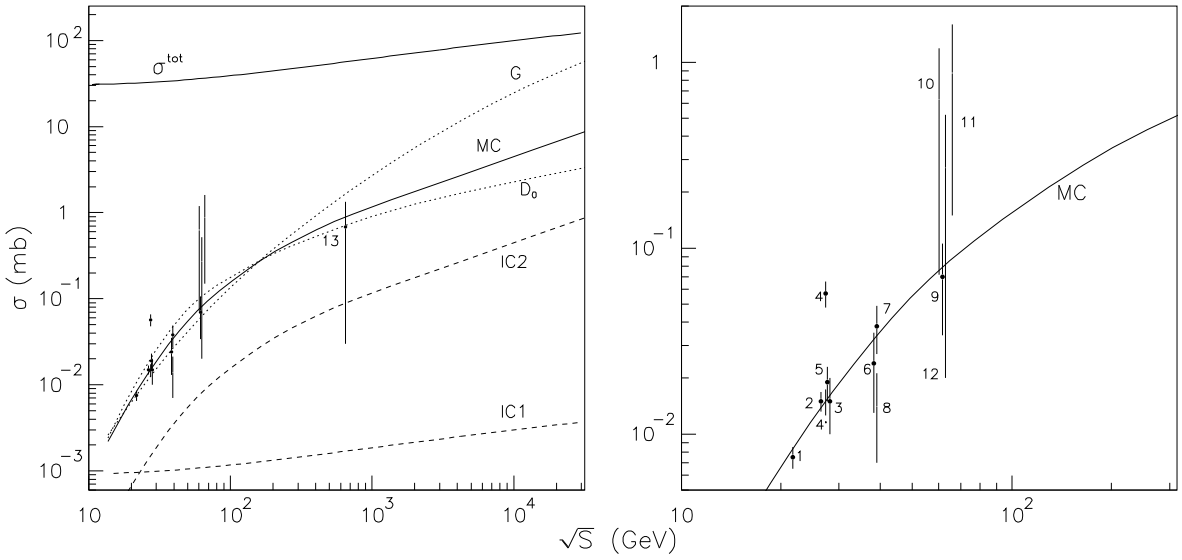

Figure 7: *Energy dependence of charm production cross section in $pp(p\bar{p})$. The experimental data points are 1:[19] 2:[20], 3:[21], 4,4':[22], 5:[23], 6:[24], 7:[25], 8:[26] 9:[27], 10:[28], 11:[29, 30], 12:[31, 30] and 13:[32]. The solid line (MC) is the result of our Monte Carlo calculations based on conventional pQCD and hadronisation, with dotted lines from variations using a naive application of the MRS parametrisations G and D_0 of parton densities in the proton. The dashed curves are from our model for intrinsic charm, with the two assumptions IC1 and IC2 about its energy dependence. For reference, the total pp cross section σ^{tot} is also shown.*

3.2 Normalisation and energy dependence of the IC cross section

As mentioned, the main uncertainty in the intrinsic charm model is the absolute normalization of the cross section and its energy dependence. Since the process is basically a soft non-perturbative one, it may be reasonable to assume that its energy dependence is the same as for normal inelastic scattering [8]. We therefore take as our first case

$$\text{IC1}: \quad \sigma_{IC}(s) = 3 \cdot 10^{-5} \sigma_{inel}(s) \tag{14}$$

shown as curve IC1 in Fig. 7 and with normalisation from ref. [9], where the magnitude of the cross section was estimated from data at relatively low energies ($\sqrt{s} = 20 - 30\,GeV$). Alternatively, one might argue that there is a stronger energy dependence related to some threshold behaviour for putting the charm quarks on their mass shell. We make a crude model for this by taking a constant fraction of the pQCD charm cross section, where such a threshold factor is included, to be our second case of the intrinsic charm cross section

$$\text{IC2}: \quad \sigma_{IC}(s) = 0.1\, \sigma_{pQCD}(s) \tag{15}$$

as shown by curve IC2 in Fig. 7. This is similar to the low energy ($\sqrt{s} = 20 - 40\,GeV$) treatment in [4]. The normalisation is fixed to be the same as IC1 at the low energy where evidence is claimed for intrinsic charm [9]. There is, however, some indication against such an increased cross section, as in IC2, since no evidence for J/ψ from intrinsic charm was found in an experiment [33] at a somewhat higher energy ($800\,GeV$ proton beam energy).

In Fig. 7 we have also compiled various data on the charm production cross section in proton-(anti)proton collisions at various energies. A few comments on the data in Fig. 7 are here in order. A given experiment is only sensitive to some channels and a limited kinematical region. The total charm cross section is therefore obtained by a rescaling with charm decay branching ratios and by using assumed shapes of the x_F distributions to extrapolate to unmeasured regions. In particular, corrections to points 1,2,6 and 7 are small while they are large for point 9 and 13. The bands 8,10,11 and 12 illustrate the uncertainties in these experiments due to this extrapolation. In band 8 the uncertainty includes a scaling for including $D^{\pm}$-mesons (taken from [24, 26]). Data-band 11 is based on $D^+\bar{D}$ identification, 12 on $\Lambda_c^+\bar{D}$ and 10 on Λ_c^+ identification. Furthermore, points 3, 4 and 5 are from beam dump experiments on heavy nuclear targets without direct charm identification and have an additional uncertainty from the scaling with nuclear number. In point 4 the scaling $A^{0.75}$ has been assumed, which we have rescaled in 4' to a A^1-dependence in order to be consistent with the other beam dump experiments and with our model [34]. Data points 2 and 6 come from pp interactions with explicit charm particle identification. Although these issues leave some uncertainty for each individual result, the combination of all data should give a trustworthy knowledge on the charm cross section and its energy dependence.

These inclusive charm cross section data can be reasonably well understood by pQCD and does not leave much room for an IC component. This follows from our detailed Monte Carlo study [34] of pQCD charm production in high energy hadron collisions based on the PYTHIA program [13] and applied to high energy cosmic ray interactions. The calculation is based on the conventional folding of the parton densities in the colliding hadrons and the leading order QCD matrix elements, for the gluon-gluon fusion process $gg \to c\bar{c}$ and the quark-antiquark annihilation process $q\bar{q} \to c\bar{c}$. Thus, the cross section is

$$\sigma = \int\int\int dx_1 dx_2 d\hat{t} \;\; f_1(x_1, Q^2)\; f_2(x_2, Q^2)\; \frac{d\hat{\sigma}}{d\hat{t}} \tag{16}$$

where x_i are the parton longitudinal momentum fractions in the hadrons and the factorisation scale is taken as $Q^2 = (m_{\perp c}^2 + m_{\perp \bar{c}}^2)/2$. The parton level pQCD cross section $\hat{\sigma}$ depends on the Mandelstam momentum transfer $\hat{t}$. Next-to-leading-order corrections are known and give a correction which can be approximately taken into account by an overall factor $K = 2$. The charm quark mass threshold $\hat{s} = x_1 x_2 s > 4m_c^2$ is important and is fully included in the matrix elements. The dominating contribution to the cross section comes from the region close to this threshold, since $d\sigma/d\hat{s}$ is a steeply falling distribution. It is therefore important to use QCD matrix elements with the charm quark mass explicitly included. The numerical value used is $m_c = 1.35\, GeV/c^2$ together with $\Lambda_{QCD} = 0.25\, GeV$ (from $MRS\,G$ [35]).

The results of this pQCD calculation is also shown in Fig. 7. At the highest energies, the parton densities are probed down to $x \sim 10^{-5}$ or even below. The recent data from HERA [36, 37] show a significant increase at small x, $xf(x) \sim x^{-a}$ and constrain the parton densities down to $x \sim 10^{-4}$. These data have been used in the parameterisation $MRS\,G$ [35] of parton densities resulting in the small-x behaviour given by the power $a = 0.07$ for sea quarks and $a = 0.30$ for gluons. This is the most recent parameterisation, using essentially all relevant experimental data and can be taken as a standard choice. The effect on the total charm production cross section from the choice of parton density parameterisation is illustrated in Fig. 7. The result is shown with $MRS\,D_0$ [38] with small-x behavior $x\,f(x) \sim const$, which before the HERA data was an acceptable parameterisation. At high energy there is a large dependence on the choice of parton density functions. The difference between the G and the D_0 parameterisations should however not be taken as a theoretical uncertainty. First of all the D_0 parameterisation is known to be significantly below the small-x HERA data and gives therefore a significant underestimate at

large energies. Secondly, the naive extrapolation of the G parameterisation below the measured region $x \gtrsim 10^{-4}$ at rather small Q^2 ($\sim m_c^2$) leads to an overestimate. A flatter dependence like $x^{-\epsilon}$ with $\epsilon \simeq 0.08$ as $x \to 0$ can be motivated ([39] and references therein) based on a connection to the high energy behaviour of cross sections in the Regge framework. The implementation of this approach in PYTHIA makes a smooth transition to this dependence such that the parton densities are substantially lowered for $x \lesssim 10^{-4}$ leading to a substantial reduction of the charm cross section at large energies, as given by the solid curve in Fig. 7.

The pQCD calculation gives a quite decent agreement with experimental charm production data over a wide range of energies. Nevertheless, the uncertainties in the data and the calculations cannot exclude some smaller non-perturbative contribution. Charm production in pQCD is theoretically well defined and has only some limited numerical uncertainty due to parameter values and NLO corrections which, however, can be examined and controlled. Non-perturbative contributions to charm production are, however, not theoretically well defined due to the general problems of non-perturbative QCD. It is therefore, reasonable to take pQCD as the main source of charm and consider, *e.g.* , intrinsic charm as an additional contribution. We show this contribution in Fig. 7 based on the two assumed energy dependences IC1 and IC2. Both cases can be consistent with the indications for IC mentioned in the Introduction, except the data in [33] which disfavours the stronger energy dependence of IC2. One should note in this context, that an even stronger energy dependence would be needed if the old ISR data were to be interpreted with intrinsic charm as the dominating source.

3.3 Charm distributions at the Tevatron and LHC

Given the differences in the pQCD and the IC mechanisms, one expects characteristic differences in the spectra of produced charmed hadrons at collider energies. Charm produced through the pQCD mechanisms should emerge with rather small longitudinal momentum or x_F. This results from the parton fusion being largest close to threshold $\hat{s} = s x_1 x_2 \sim 4m_c^2$. In contrast, intrinsic charm is giving rise to charm particles at large fractional momenta relative to the beam particles, as explained before. The latter process may therefore dominate at some large x_F, with the cross-over point depending on the relative normalisations of the cross sections for the two processes.

To study this, we have used our models and calculated the spectra in x_F and rapidity of charmed hadrons at the Tevatron and LHC shown in Figs. 8 and 9. Only one hemisphere ($x_F > 0, y > 0$) is shown, corresponding to the proton beam direction at the Tevatron, such that the other hemisphere is obtained with charge conjugation symmertry. Since the pQCD processes are fully Monte Carlo simulated one can easily extract the x_F and rapidity $y = ln\{(E + p_z)/(E - p_z)\}$. Our model for intrinsic charm is analytic and formulated in terms of x_F-dependencies. The rapidity is then calculated using $y \simeq ln\,(2x_F P/m_\perp)$, with P the beam momentum and $m_\perp$ the transverse mass of the charmed hadron. As usual in IC models, we neglect the transverse momentum although it may be expected to be of the same order as the charm quark mass. Including $p_\perp$ fluctuations of this magnitude, would only cause shifts to lower rapidity of about $ln(\sqrt{2}) \simeq 0.35$ which is significantly smaller than the widths of the rapidity peaks in Fig. 9 and therefore not change the results significantly.

In comparison to the Tevatron, the charm cross section at LHC is larger by a factor four for pQCD and IC2 and a factor two for IC1. The IC distributions essentially scale in x_F, but shift to larger rapidity at LHC due to the higher beam momentum. The increase for pQCD is mainly at small x_F, due to the charm threshold moving to smaller momentum fractions x in the colliding particles.

With the stronger energy dependence of IC2, the IC cross section is significantly higher than

that from pQCD at large longitudinal momentum. The milder energy dependence of IC1 gives a charm cross section which is in general much smaller than the pQCD one and cannot really compete even at high x_F. The only exception is for $\overline{D}$ where the previously discussed leading particle effects are important, resulting in cross sections of similar magnitude as pQCD for very large x_F or rapidity. Thus, it is will be very hard to test the IC1 case, but the IC2 case could be observable provided that the forward coverage of the detectors is extended far enough. This could be considered in connection with dedicated heavy flavour experiments covering the forward region in particular.

4 Summary and conclusions

The hypothesis of intrinsic charm quark-antiquark pairs in the proton wave function is not ruled out by experiment. On the contrary, there are some evidence in favour of it, but no safe conclusion can be made at present. It is therefore important to consider various ways to gain additional information that could help clarify the situation. Based on previous work, we have constructed explicit models for intrinsic charm and how it may be examined in deep inelastic lepton-nucleon scattering and hadron collisions. Our models are partly implemented in terms of Monte Carlo programs, which allow detailed information to be extracted since complete events are simulated.

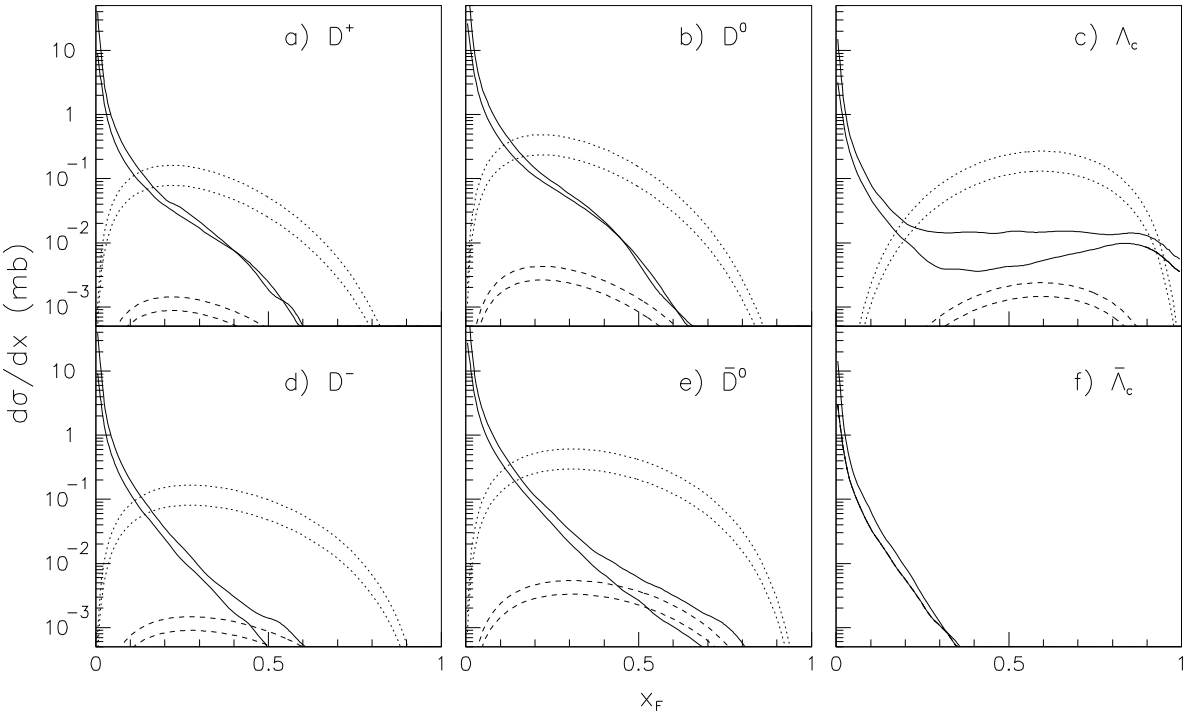

Figure 8: *Cross section versus longitudinal momentum fraction x_F for charm particles produced from pQCD (full curves) and from the intrinsic charm model with energy dependence IC1 (dashed curves) and IC2 (dotted curves). In each case, the upper curves correspond to LHC (pp at $\sqrt{s} = 14\,TeV$) and the lower ones to the Tevatron ($p\bar{p}$ at $1.8\,TeV$). Only one hemisphere $x_F > 0$ (proton beam direction) is given.*

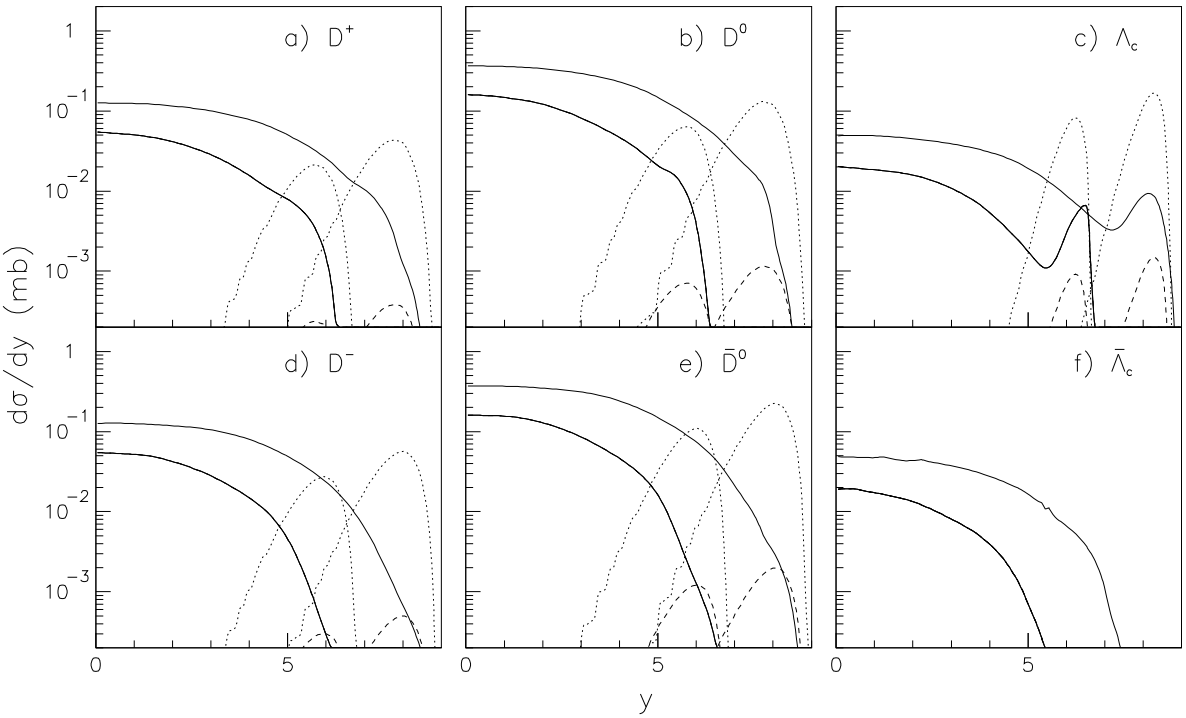

Figure 9: *Cross section versus rapidity for charm particles produced from pQCD (full curves) and from the intrinsic charm model with energy dependence IC1 (dashed curves) and IC2 (dotted curves). In each case, the upper curves correspond to LHC (pp at* $\sqrt{s} = 14\,TeV$*) and the lower ones to the Tevatron (*$p\bar{p}$ *at* $1.8\,TeV$*). Only one hemisphere* $y > 0$ *(proton beam direction) is given.*

In DIS such intrinsic charm quarks can be directly probed and we find that it may dominate the inclusive charm F_2^c structure function at large x. Muons from charm decay can be used to signal events with charm and we compare results of the IC mechanism with the conventional perturbative QCD boson-gluon fusion process, as well as background muons from π and K decays. We devise cuts in order to enhance IC relative to the backgrounds. Signal and backgrounds can then be brought to about the same level. We point out that data samples already collected by NMC would be suitable for this purpose and could be sensitive down to a level of about 0.2% probability of intrinsic charm in the proton.

Direct scattering on intrinsic charm quarks at HERA has been investigated before [10]. Here, we investigate the indirect process with scattering on a light valence quark such that the $c\bar{c}$ fluctuation in the proton remnant is realised. The rapidities of the produced charmed particles have been calculated and found to be very forward, as expected. Present detectors do not have enough forward coverage to detect these processes, but one may consider them in connection with possible upgrades for future HERA running.

For hadronic interactions, the intrinsic charm model gives definite predictions for charmed particle x_F spectra. The absolute normalisation and its energy dependence is, however, not clear. We have investigated this in comparison with conventional pQCD productions mechanism for charm and measured charm production cross sections. This constrains the allowed energy variation of the IC cross section. Using two simple models for this energy dependence, we calculate the x_F and rapidity distributions for charmed particles at the Tevatron and LHC. We

find that it is only if the IC cross section has a significant rise with energy, that it can compete with normal pQCD production of charm. In any case, the IC contribution is at very large forward momenta, such that its detection would require coverage at very forward rapidities.

In the context of very high energy hadronic collisions one should also consider cosmic ray interactions in the atmosphere, which we have investigated in detail [34]. Here also, the intrinstic charm mechanism would contribute significantly only if it has a strong energy dependence.

Finally, one should remember the possible extension from intrinsic charm to intrinsic bottom quarks. Although we have not presented numerical results, our methods can easily be applied for intrinsic bottom processes. In comparison to charm the general expectations are, as discussed in the Introduction, that the x_F-distributions will be only slightly harder but the overall rates lower by about a factor ten.

Acknowledgements: We are grateful to S. Brodsky for helpful communications and to J. Rathsman for a critical reading of the manuscript.

References

[1] S.J. Brodsky, P. Hoyer, C. Peterson and N. Sakai, Phys. Lett. **B93** (1980) 451; S.J. Brodsky and C. Peterson, Phys. Rev. **D23** (1981) 2745.

[2] R. Vogt and S.J. Brodsky, Nucl. Phys. **B438** (1995) 261.

[3] R. Vogt and S.J. Brodsky, *Charmed Hadron Asymmetries in the Intrinsic Charm Coalescence Model*, SLAC-PUB-95-7068, LBL-37666.

[4] R. Vogt, S.J. Brodsky and P. Hoyer, Nucl. Phys. **B360** (1991) 67.

[5] R. Vogt and S.J. Brodsky, Phys. Lett. **B349** (1995) 569.

[6] E. Hoffmann and R. Moore, Z. Phys. **C20** (1983) 71.

[7] B.W. Harris, J. Smith and R. Vogt, Nucl. Phys. **B461** (1996) 181.

[8] S.J. Brodsky *et al.*, Nucl. Phys. **B369** (1992) 519.

[9] R. Vogt, S.J. Brodsky and P. Hoyer, Nucl. Phys. **B383** (1992) 643.

[10] G. Ingelman, L. Jönsson and M. Nyberg, Phys. Rev. **D47** (1993) 4872.

[11] G. Ingelman, J. Rathsman and A. Edin, LEPTO 6.4 – A Monte Carlo for Deep Inelastic Lepton-Nucleon Scattering, DESY preprint, to appear.

[12] B. Andersson, G. Gustafson, G. Ingelman and T. Sjöstrand, Phys. Rep. **97** (1983) 33.

[13] T. Sjöstrand, PYTHIA 5.7 & JETSET 7.4, Comput. Phys. Commun. **82** (1994) 74

[14] G. Ingelman, J. Rathsman and G.A. Schuler, AROMA 2.2 – A Monte Carlo Generator for Heavy Flavour Events in *ep* Collisions, DESY preprint, to appear.

[15] J.J. Aubert *et al.*, Phys. Lett. **110B** (1982) 73; Nucl. Phys. **B213** (1983) 31.

[16] M. Thunman, *Searching for Heavy Quarks at NMC: A Simple Estimate of Background Muons from π and K decays*, Uppsala preprint TSL/ISV-96-0138.

[17] S. Brodsky, W.-K. Tang, P. Hoyer, Phys. Rev. **D52** (1995) 6285

[18] C. Petersson *et al.*, Phys. Rev. **D27** (1983) 105.

[19] P. E. Karchin, E769 Collaboration, *Current Issues in Open Charm Hadroproduction and New Preliminary Results from Fermilab E769*, FERMILAB-Conf-95/053-E.

[20] M. Aguilar-Benitez *et al.*, Phys. Lett. **B189** (1987) 476.

[21] M. Jonker *et al.*, Phys. Lett. **96B** (1980) 435.

[22] M. E. Duffy *et al.*, Phys. Rev. Lett. **57** (1986) 1522.

[23] P. Fritze *et al.*, Phys. Lett. **96B** (1980) 427.

[24] R. Ammar *et al.*, Phys. Rev. Lett. **61** (1988) 2185.

[25] K. Kodama *et al.*, Phys. Lett. **263B** (1991) 573.

[26] M. J. Leitch *et al.*, Phys. Rev. Lett. **72** (1994) 2542.

[27] A. G. Clark *et al.*, Phys. Lett. **77B** (1978) 339.

[28] P. Chauvat *et al.*, Phys. Lett. **B199** (1987) 304.

[29] M. Basile *et al.*, Nuovo Cimento **67A** (1982) 40.

[30] A. Contin *et al.*, in *Int. Conf. on High Energy Physics,* Lisbon 1981, eds. J. Dias de Deus and J. Soffer, p. 835.

[31] G. Bari *et al.*, Nuovo Cimento **104A** (1991) 571.

[32] O. Botner *et al.*, Phys. Lett. **B236** (1990) 488.

[33] M. S. Kowitt *et al.*, Phys. Rev. Lett. **72** (1994) 1318.

[34] M. Thunman, G. Ingelman and P. Gondolo, *Charm Production and High Energy Atmospheric Muon and Neutrino Fluxes* Uppsala preprint TSL/ISV-95-0120 (revised February 1996), hep-ph/9505417.

[35] A. Martin, R. Roberts and J. Stirling, Phys. Lett. **B354** (1995) 155.

[36] H1 Collaboration: I. Abt *et al.*, Nucl. Phys. **B407** (1993) 515; T. Ahmed *et al.*, NuclPhys. **B439** (1995) 471.

[37] ZEUS Collaboration: M. Derrick *et al.*, Phys. Lett. **B316** (1993) 412; Z. Phys. **C65** (1995) 379, Phys. Lett. **B345** (1995) 576.

[38] A. Martin, R. Roberts and J. Stirling, Phys. Lett. **B306** (1993) 145.

[39] G.A. Schuler and T. Sjöstrand, Nucl. Phys. **B407** (1993) 539.